A Wideband Fully Integrated Software-Defined Transceiver for FDD and TDD Operation

Hazal Yüksel, *Student Member, IEEE*, Dong Yang, Zachariah Boynton, Changhyuk Lee, *Member, IEEE*, Thomas Tapen, Alyosha Molnar, *Member, IEEE*, and Alyssa Apsel, *Senior Member, IEEE*

***Abstract*— Although there is much active research on software-defined radios (SDRs) with receive (RX) or transmit (TX) functionality, little work has been done on SDR transceivers supporting frequency division duplex (FDD). In this paper, we present a new circuit concept in which a distributed TX circuit cancels the transmitted signal at a reverse RX port through destructive interference while adding signal constructively at a forward TX port. We pair the distributed transmitter with a receiver-tracking PA degeneration technique to suppress the injected noise from TX circuits in the RX band. The system does not require off-chip filters or circulators, but still achieves both SDR flexibility and both FDD and time division duplex function. Measurements from the transceiver implemented in 65-nm CMOS show a frequency tuning range of 0.3–1.6 GHz with TX–RX isolation >23 dB and transmitted power up to 19 dBm.**

***Index Terms*— distributed amplifier, duplexer, flexible, passive mixer, software-defined, transceiver, transmission line, transmit-receive isolation.**

I. Introduction

MOST modern wireless systems must support duplex communications [i.e., frequency division duplex (FDD) and time division duplex (TDD)], and be able to access an ever increasing range of frequencies and standards. This latter requirement has generated interest in dynamic and scalable spectrum access, which has driven research on flexible, software-defined receivers [1]–[5] and transmitters [6]. Although there has been progress in developing RFICs to enable radios with either integrated duplex operation [7]–[11], [26], [27] or high flexibility, a fully integrated radio combining both features with high TX output power has yet to be demonstrated.

Limited spectrum availability in two-way commercial radio (i.e., GSM 900/1800, 4G-LTE) has created such demand that auctions for the 700-MHz band generated U.S. $19 billion in 2008 [12]. To address this, the FCC has adopted reverse-auctioning, buying back TV bands, and opening up spectrum in a fragmented fashion [12]. Transceivers that use frequency inflexible elements, such as high-Q filters (i.e., SAW and BAW filters), diplexers, circulators, and/or TR switches, have a limited ability to use these new bands.

Manuscript received August 23, 2016; revised November 21, 2016; accepted December 27, 2016. Date of publication January 27, 2017; date of current version April 20, 2017. This paper was approved by Guest Editor Danilo Manstretta. (H. Yüksel and D. Yang contributed equally to this work.)

H. Yüksel, Z. Boynton, C. Lee, T. Tapen, A. Molnar, and A. Apsel are with Cornell University, Ithaca, NY 14853 USA (e-mail: hy434@cornell.edu).

D. Yang is with Cypress Semiconductor Corporation, San Jose, CA 95134 USA.

Color versions of one or more of the figures in this paper are available online at http://ieeexplore.ieee.org.

Digital Object Identifier 10.1109/JSSC.2017.2650409

Meanwhile, FDD is used in most licensed bands for cellular communication worldwide, and offers reduced latency relative to TDD. FDD enables full data capacity for both transmit and receive, meaning that FDD deployments provide greater coverage and can achieve cell edge rates further from the base station (∼5 dB better [13]), requiring fewer base stations, reducing cost. Current FDD implementations tend to employ symmetric up- and down-link channels, and so suffer when data rates flowing on the downlink exceed the uplink, degrading spectral efficiency compared with TDD. However, this assumes fixed equal bandwidths for both links, an assumption that is likely to change with the deployment of a true software-defined radio (SDR) FDD. Nonetheless, the benefits of FDD have been significant enough to outweigh the challenges that FDD imposes on the radios themselves.

To support FDD, a transceiver must separate receive (RX) and transmit (TX) signals. A typical FDD duplexer can be treated as a 3-port network, with a TX port, RX port, and antenna port. Strong TX signals must be delivered to the antenna without compressing, saturating, or damaging the receiver. At the same time, TX and RX should not load each other, as this will degrade TX efficiency and increase RX loss as RX signals pass from antenna to RX port. Similarly, TX noise in the RX band should be suppressed at the RX input to avoid desensitizing the receiver. Finally, this isolation should be maintained in the presence of changing antenna impedance.

Commercial duplexers rely on linear passive structures, typically filters (i.e., SAW and BAW) or circulators/magnetic structures, between receive and transmit circuits to provide TX–RX isolation. These techniques are narrowband, inflexible in frequency, and difficult to integrate with circuitry, requiring banks of low noise amplifier (LNAs), PAs, and off-chip elements for multiband function [1]. Integrating these functions using "electrical balance" structures, incurs intrinsic losses (on the order of 5 dB) with a relatively narrow, inflexible band [6], [14]–[16]. Recently developed circulator and duplexer circuits avoid fundamental losses, but are limited in bandwidth and TX power [17], [18]. Finally, employing multiple antennas to achieve isolation [7], [8], [10], [15] increases system size, and/or uses multiple antennas that could be better used for MIMO operation. Furthermore, most SDR/full-duplex radio efforts involve multiple antennas with antenna duplexing chips, and there exist only a few works that integrate the antenna interface on chip [14]–[17].

In this paper, we present a circuit that combines two new techniques into a programmable transceiver capable of

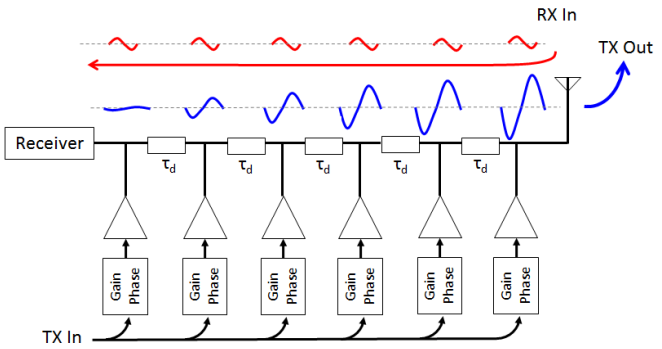

Fig. 1. Concept for distributed duplexing transceiver. $N_{\rm st} = 6$ sub-PAs apply weighting (gain and phase shift) to TX input and inject into an artificial TL made of segments with delay τ_d. TX signals add constructively at the antenna and null at the receiver. Received signals from the antenna propagate to the receiver.

flexible FDD (as well as TDD) operation across a wide range of frequencies on a single antenna. The transmitter is composed of a distributed array of smaller subtransmitters with programmable gain and phase, each of which is coupled into an artificial transmission line (TL). Careful choice of gain and phase of each subtransmitter output allows signal power to combine in the forward direction and cancel at the reverse port, as demonstrated in [19] and [20]. Noise injected by the PAs into the line is suppressed using an RX tracking degeneration scheme that selectively reduces PA transconductance in the RX band. This, combined with a passive mixer first receiver, allows simultaneous transmit and receive across a wide frequency range for software-defined FDD.

This paper is organized as follows. In Section II, we discuss the fundamental concept and the core ideas of the transceiver. In Section III, we present the detailed subcircuits, and discuss design tradeoffs. In Section IV, we present measurement results that characterize the individual system components as well as the FDD function of the system as a whole.

II. Key Techniques and System Architecture

The presented software-defined FDD transceiver employs two critical circuit techniques as well as an overall system architecture to support them, all of which are discussed here.

A. Distributed Duplexing Structure

To protect the receiver from large TX signals without unduly loading the TX, we propose the distributed structure shown in Fig. 1. The antenna and RX ports are separated by an artificial TL made up of inductors and capacitors, which provides an electrical delay and allows RX signals to pass from the antenna port to the RX port with low insertion loss. A distributed transmitter consisting of $N_{\rm st} = 6$ subtransmitters injects currents into different taps along the TL. The subtransmitters are driven by the same upconversion local oscillator (LO) and baseband input signal, while the amplitude and phase of each subtransmitter output is independently controlled by its baseband circuitry, acting as a complex valued weight between the TX input and each injection point. As with a traditional distributed amplifier, the TX signals can be made to add in phase along the TL to deliver a strong signal to the antenna port. However, full control of the complex weight of each subtransmitter allows the TX signal to be simultaneously nulled at the RX port.

1) Mathematical Foundation for TX–RX Isolation Using a Distributed TX Circuit: In order to choose appropriate weights to achieve these goals, we first model the TL as an $N_{\rm st}$-terminal impedance matrix $Z_{\rm TL}$. The matrix $Z_{\rm TL}(\omega)$ incorporates the complex impedances of the component inductors and capacitors, series and shunt resistive losses, and the termination impedances of the receiver and antenna, as shown in Fig. 2. The subtransmitters inject $N_{\rm st}$ currents $(i_1, i_2, \ldots, i_{N_{\rm st}})$, each proportional to the global TX input, $V_{\rm in,TX}$, times a local complex weight, such that $i_i = V_{\rm in,TX} y_{\rm mi}$, where $y_{\rm mi}$ is the transadmittance of the ith subtransmitter, incorporating its complex weight. These currents interact with the TL (characterized by the $Z_{\rm TL}$ matrix) to generate $N_{\rm st}$ voltages. We are only concerned with two of these voltages: the voltage at the antenna port, $V_{\rm ant} = V_1$, and the voltage at the RX port, $V_{\rm RX} = V_{N_{\rm st}}$. The requirements for FDD can be formulated in matrix form

$$\begin{pmatrix} V_{\rm ant} \\ V_{\rm RX} \end{pmatrix} = \vec{v} = Z(\omega_{\rm TX})\vec{y_m} V_{\rm inTX} \tag{1}$$

where $Z(\omega_{\rm TX})$ relates the $N_{\rm st}$ injected currents to the two endpoint voltages at the TX frequency. For a 50-Ω TL with matched termination impedances, $Z(\omega)$ can be approximated as

$$Z(\omega) = 25\Omega \begin{bmatrix} 1 & \alpha \cdot e^{j\omega\tau_d} & \cdots & (\alpha \cdot e^{j\omega\tau_d})^{N_{\rm st}-1} \\ (\alpha \cdot e^{j\omega\tau_d})^{N_{\rm st}-2} & (\alpha \cdot e^{j\omega\tau_d})^{N_{\rm st}-1} & \cdots & 1 \end{bmatrix} \tag{2}$$

where τ_d is the per stage delay and α is the per stage loss ($\alpha < 1$) due to finite inductor Q and PA output impedance. However, the analyses presented here hold even when $Z(\omega)$ deviates from (2) due to impedance mismatch or lumped-element effects.

The goal is to find the $N_{\rm st}$-entry weight-vector, $\vec{y_m}$ that generates the desired voltage at the antenna $V_{\rm ant} = A_{v,\rm PA} V_{\rm in}$ while nulling it at the receiver $V_{\rm RX} = 0$, accomplishing duplex. For $N_{\rm st} > 2$, many solutions exist to meet these two restrictions, but a desirable solution also minimizes the magnitude of the injected currents, and so the weights, allowing minimization of bias currents and therefore increased array efficiency. Applying the pseudoinverse gives

$$\vec{y_m} = Z^*(ZZ^*)^{-1} \begin{pmatrix} A_{v,\rm PA} \\ 0 \end{pmatrix} \tag{3}$$

where Z^* is the Hermitian of Z. This is the unique solution that minimizes the summed-squared current while generating the required terminal voltages.

The finite bit resolution (N) of the complex weights $\vec{y_m}$, can limit cancellation, as imperfect weights result in an imperfect null at the RX port. Ideally, cancellation is upper-bounded to 2 dB + 6 dB(N) + 10log$(N_{\rm st} - 1)$. In this design, we chose

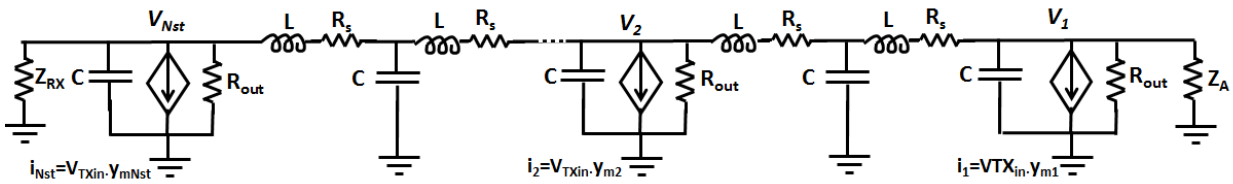

Fig. 2. Linear circuit model of distributed duplex transceiver. TL segments composed of *LC* T-sections (with parasitic resistance R_S). PAs are modeled as current sources injecting weighted versions of the input.

$N_{\rm st} = 6$, and $N = 7$ b, setting an upper limit on rejection of 50 dB.

2) Tradeoffs of the Transmission Line Design Parameters: The two main parameters that define the frequency range of the distributed transmitter are the interstage delay of the TL, τ_d, and the number of stages, $N_{\rm st}$. Although, in theory, both perfect rejection and arbitrary output power can be supported at all nonzero frequencies, the efficiency becomes unacceptable outside a certain range of frequencies. For frequency approaching $1/(2\tau_d)$ at the high end and below $1/(4N_{\rm st}\tau_d)$ at the low end, efficiency becomes significantly degraded, making reasonable operation unfeasible. Thus, $N_{\rm st}$ sets the range of frequencies that are reachable as $f_{\rm max}/f_{\rm min} \approx 2N_{\rm st}$, while the per-stage delay τ_d sets the upper frequency limit. Other limits on performance include the loss from inductors and capacitors, TL cutoff frequency, and the finite output impedance of the individual PAs. As diagramed in Fig. 2, the system can be modeled as alternating series inductors and shunt capacitors, with loss associated with inductors modeled as series resistance $R_S = L\omega/Q$. It can be shown that the total loss from R_S is equal to $N_{\rm st}\tau_d\omega/Q$, favoring a shorter TL. Each subtransmitter is modeled as a controlled transadmittance in parallel with output resistance $R_{\rm out}$ and capacitance C. While the output capacitance of the subtransmitters can be absorbed into the TL itself, the output resistance is lossy, which we address with PA degeneration.

B. RX-Tracking PA Degeneration

The noise coming from the shared baseband circuits is correlated and filtered, and, similarly, the TX and RX LO noise sources are also correlated and, therefore, are suppressed by the distributed suppression. However, the noise generated by the subtransmitters themselves is not correlated and therefore cannot be suppressed by the distributed duplexing that cancels the correlated TX signals at the RX port. The uncorrelated noise comes from both the common source stage of the PA itself ($\overline{i_n^2} = 4{\rm kT}\gamma\, g_{m,{\rm PA}}$), and from preceding RF and baseband circuits ($\overline{i_n^2} = \overline{v_{n,{\rm TX}}^2} g_{m,{\rm PA}}^2$), where $\overline{v_{n,{\rm TX}}^2}$ is the noise of all TX stages before the PA. Noise from the combined $N_{\rm st}$ subtransmitters will therefore degrade the NF at the RX port by at least

$$\text{NF} > 10\log\left(1 + \gamma\, N_{\rm st} A_v + N_{\rm st}\frac{\overline{v_{n,{\rm TX}}^2} A_v^2}{4{\rm kTR}_L}\right) \tag{4}$$

where $A_v = g_{m,{\rm PA}} R_L$ is the voltage gain of a single PA, and R_L is the parallel impedance of the two ends of the TL, typically 25 Ω. Thus, for a composite voltage gain $V_{\rm out}/V_{\rm in\cdot TX} \approx 10$, NF > 10 dB just from the PAs themselves, excluding all other noise sources.

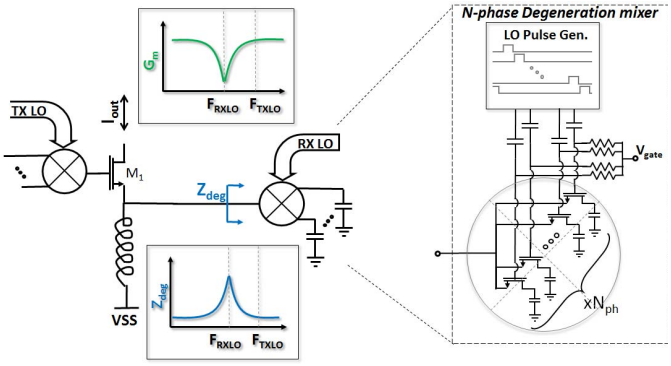

Fig. 3. RX-tracking PA degeneration. Left: concept, common source amplifier (M_1) is degenerated by an inductor in parallel with a passive mixer. The mixer is a high impedance near $f_{\rm RX,LO}$, but low elsewhere, including $f_{\rm TX,LO}$. The effective transconductance of the amplifier is notched at $f_{\rm RX,LO}$. Right: implementation of $N_{\rm ph}$ phase mixer with LO pulses ac-coupled to gates.

Because this noise is intrinsically related to the gain of the transmitter, it cannot simply be suppressed through careful design of standard transmitter circuits. Preventing this noise from desensitizing the receiver without destroying transmitter function requires selectively suppressing the PAs' gain in the RX band relative to the TX band.

To suppress the transmitter's noise and boost its output impedance in the RX band, we employ a passive mixer-based PA degeneration scheme to provide a high, narrow-band degeneration impedance at the RX frequency, as shown in Fig. 3. A passive mixer is connected to the source of each PA's common source device, in parallel with a large-value dc choke for bias current. The mixer's baseband port is loaded by large capacitors, and its LO port is driven by the RX LO signal of frequency $\omega_{\rm RX}$.

From [21], an $N_{\rm mix}$-phase passive mixer presents a bandpass impedance centered at $\omega_{\rm RX}$

$$Z_{\rm deg} = R_{\rm sw} + \frac{R_{\rm sw} + R_{\rm sc}}{1 - \text{sinc}^2(\pi/N_{\rm mix})} \Bigg\| \frac{\text{sinc}^2(\pi/N_{\rm mix})}{j|\omega_{\rm in} - \omega_{\rm RX}|C_L N_{\rm mix}}. \tag{5}$$

Here, $R_{\rm sw}$ is the ON resistance of the passive mixer switches and $R_{\rm sc}$ is the source impedance looking out of the passive mixer's RF port, or roughly $1/g_{m1}$. Analysis of (5) shows that when $|\omega_{\rm in} - \omega_{\rm RX}| \gg 0$, the input impedance of the degeneration mixer is $Z_{\rm deg} = R_{\rm sw}$. But when $\omega_{\rm in} \approx \omega_{\rm RX}$,

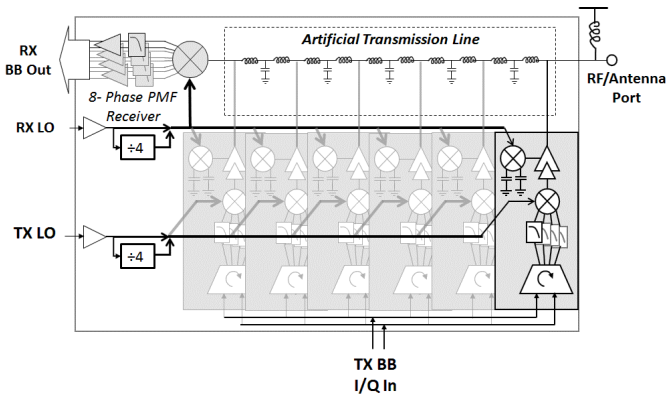

Fig. 4. System block diagram. TX LO and baseband signals are distributed to six subtransmitters, each with independent complex gain, upconversion, and degenerated PA. TX cells are coupled into *LC* passive delay line, connecting the antenna port and receiver. The RX LO is distributed to the receiver and TX degeneration mixers.

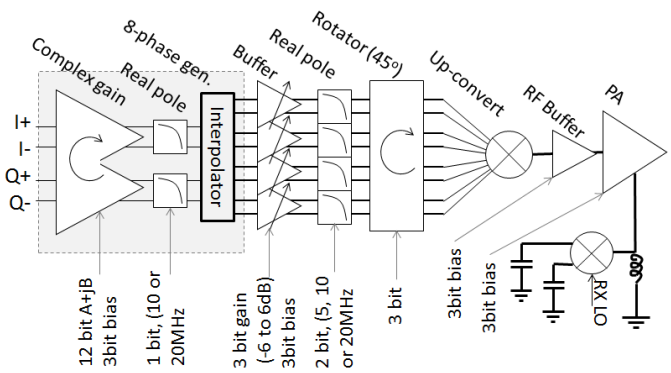

Fig. 5. Details of subtransmitter design, showing controls for gain, bandwidth, rotation angle, and current bias.

the input impedance in the RX band increases to

$$Z_{\rm deg}(\omega_{\rm RX}) = R_{\rm sw} + (R_{\rm sw} + R_{\rm sc})/(1 - {\rm sinc}^2(\pi/N_{\rm mix})). \quad (6)$$

The composite transconductance of the PA is reduced by $Z_{\rm deg}$ to be $G_{m,{\rm PA}} = (g_{m1}/1 + g_{m1}Z_{\rm deg}(\omega))$, so that the bandpass degeneration impedance produces a band-notch PA transconductance, as shown in Fig. 3. Substituting in $Z_{\rm deg}$ from (5), and assuming $|\omega_{\rm TX} - \omega_{\rm RX}| \gg (R_{\rm sw} + g_{m1})N_{\rm mix}C_L$, the relative amount of degeneration between RX and TX bands is

$$A_{\rm deg} = \frac{G_{m,{\rm PA}}(\omega_{\rm RX})}{G_{m,{\rm PA}}(\omega_{\rm TX})} \approx (1 - {\rm sinc}^2(\pi/N_{\rm mix})). \quad (7)$$

For $N_{\rm mix} = 8$, this implies an ideal $A_{\rm deg} \approx 1/19.8 \approx -26$ dB. Since gain terms A_v are reduced by this factor of $A_{\rm deg}$, the RX-band NF is substantially reduced with much less impact on the TX-band gain.

This degeneration technique also increases the output impedance of the subtransmitter PAs', $R_{\rm out}$ by a factor of $1/A_{\rm deg}$ in the RX band. Since $R_{\rm out}(\omega_{\rm RX})$ acts as a shunt loss mechanism, attenuating incoming RX signals by $-N_{\rm st}20\log(1 + R_L/R_{\rm out}(\omega_{\rm RX}))$ dB, increasing $R_{\rm out}$ by $1/A_{\rm deg}$, greatly mitigates shunting RX loss.

C. Impact of Techniques on Various Noise Mechanisms

Although the techniques proposed earlier mitigate noise degradation of the RX by the TX, careful design of the various subblocks shown in Fig. 4 is still required to avoid excessive RX-band noise from the various TX elements. TX noise sources in this design are subject to one or more of the following mitigating mechanisms.

1) Any noise mechanism introduced in the transmitter before upconversion will be subject to at least one pole of low-pass filtering in the TX baseband, suppressing it in the RX band.
2) Any noise mechanism that maps to a voltage on the gate of the PA core device will be subject to the RX LO tracking degeneration. This includes noise from baseband, upconversion, and RF preamplification circuits, all suppressed by a factor of $A_{\rm deg}^2$, and PA noise, suppressed by a factor of $A_{\rm deg}$. It also includes phase noise present on the TX LO, suppressed by factor of $A_{\rm deg}^2$.
3) Finally, noise that is correlated across transmitters is suppressed by a factor $A_{\rm dist}(\omega) \approx |\omega - \omega_{\rm TX}|/\omega_{\rm TX}$ reflecting the fact that subTX gains are weighted to cancel at the RX port of the TL. This includes any noise present on the TX baseband inputs (from DAC quantization noise, for example). It also includes the LO phase noise common to all six transmitters. This applies not just to the TX LO phase noise, but also to the RX LO phase noise. Phase noise in the RX LO, at the TX frequency, acts through the degeneration mixers to downconvert the TX signal to near dc. The mixers then reupconvert this signal into the RX band, generating the RX-band noise proportional to the TX signal and RX LO phase noise. But this noise is correlated across subtransmitters and proportional to sub-TX signals' magnitude and phase, so it is suppressed similar to the TX signal.

III. Circuit and Subsystem Design

The full system is shown in Fig. 4. A six-stage distributed transmitter was implemented with five TL segments. Each subtransmitter (details in Fig. 5), comprises a one-quadrant baseband rotator followed by a four-to-eight phase interpolator, a 45° resolution four-quadrant rotator, eight-phase passive upconversion mixer, RF preamplifier, and degenerated PA. Up-conversion and degeneration mixers are driven by shared LO signals. These shared LO signals are generated by global RX and TX LO blocks and are locally retimed (further explained at Section III-E) at each subtransmitter. The RX LO also drives the RX down conversion mixer.

Because signal level builds up along the TL, as shown in Fig. 1, PAs close to the RX see much smaller signals than those close to the antenna port. Ideally, the supply rails would be stepped up linearly along the length of the TL in proportion to the signal level to maximize system efficiency. In this design, we compromised with two VSS supply rails (GND and VSS PA) as shown in Fig. 6, eliminating 50% of the wasted power lost in a single supply design.

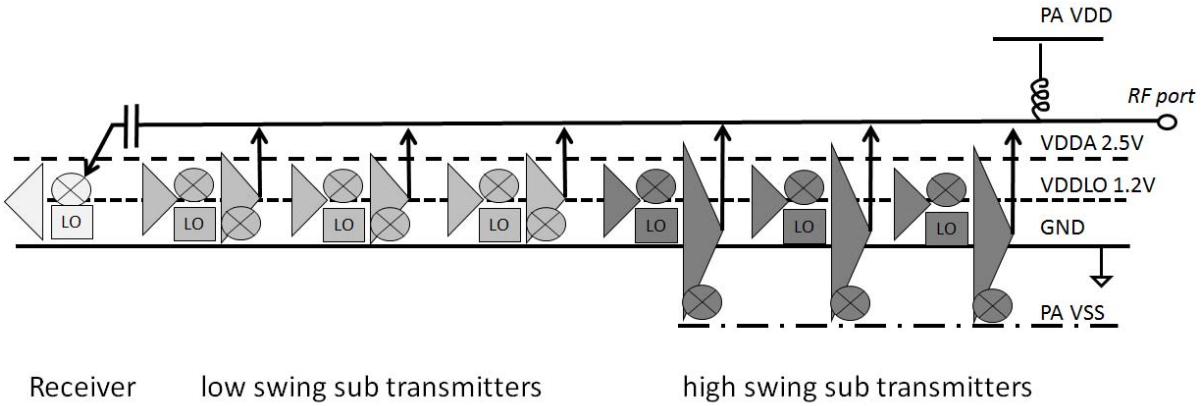

Fig. 6. Power supply distribution: LO and analog circuits were supplied by 1.2 and 2.5 V, respectively. High swing PAs were supplied with a VSS below GND (−2.5 V), and the main TL was biased through an off-chip choke to the PA VDD (2.5 V).

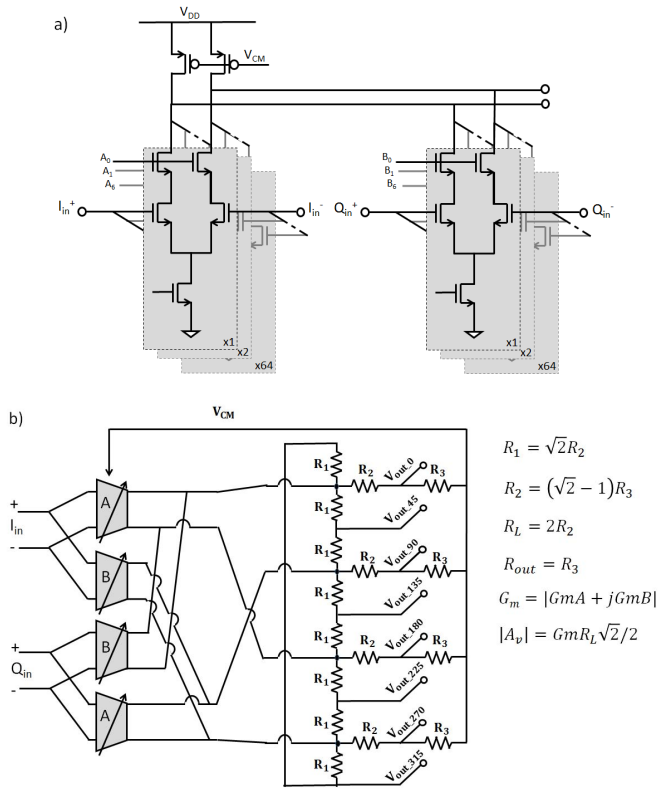

Fig. 7. Interpolator. (a) One-quadrant I–Q interpolator: banks of unit differential pairs provide real and imaginary transconductance terms with magnitudes A and B. (b) Four-to-eight phase interpolating resistive network, with the given values for R_1, R_1, and R_1, presents a differential load to the I and Q transconductance from (a) and generates equal magnitude, 45° rotated output voltages each with output resistance $R_{\text{out,BB}}$.

A. Complex-Weighted Programmable TX Baseband

The TX baseband starts with an interpolator, as shown in Figs. 5 and 7, to combine the I and Q inputs so that $I_{\text{out}} = \text{AV}_I + \text{BV}_Q = M\cos(\omega_{\text{BB}}t + \theta)$. With the correct choice of A and B, implemented by binary-weighted programmable input differential pairs as shown in Fig. 7(a), an output with constant amplitude and a specific phase between 0° and 90° can be generated.

A resistor network is added to further interpolate the four-phases to eight-phases with 45° phase splitting. By choosing the resistor values correctly, as shown in Fig. 7(b), this interpolating load provides matched output resistances and signal amplitudes at all eight output ports. Note that this circuit operates similar to a harmonic rejection circuit, so that errors in resistor ratios result in unwanted third-harmonic upconversion proportional to the magnitude of the error. A capacitive load filters all eight outputs for noise. The first two stages generate programmable phase delay between 0° and 90°, while phase shifts from 0° and 360° is required. Fortunately, the eight-phase signals inherently provide 45° phase splits and so after a second round of buffering and filtering, eight 8:1 analog MUXes were used to map the eight baseband outputs to the eight inputs of the upconversion mixer, providing an arbitrary phase shift by any multiple of 45°.

B. TX RF Circuits: Upconversion, Preamplifier, PA

Once the TX baseband signals are weighted, filtered, and interpolated to eight phases, they must be upconverted independently in each subtransmitter. An eight-phase passive mixer upconverts the signal, both to take the advantage of low noise of such structures, and to suppress upconversion to the second through sixth harmonics.

One downside to this approach is the limited signal amplitude that passive mixers can support. This small signal swing requires inclusion of an RF preamplifier before the output (PA) stage. The preamplifier is a simple, resistively loaded common-source amplifier with a gain of 2.5 (8 dB) and output swing up to $2V_{\text{pp}}$. The expected output noise of the mixer and preamplifier must be kept low to avoid desensitizing the receiver, even when suppressed by A_{deg}^2. $R_{\text{sw,mix}}$ was designed to be ∼7 Ω, $R_{L,\text{pre}} = 20$ Ω, and so $g_{m,\text{pre}} = 125$ mS.

The output stages (“PAs,” shown in Fig. 8) of each subtransmitter achieve several conflicting goals at once. The first is to provide stand-alone voltage gain with low noise. Each stage achieves a voltage gain of approximately 2 (6 dB), so as to provide a composite voltage gain across all six stages of about 10, accounting for TL loss. Since the TX line presents a load of 25 Ω to the PA (50 Ω from each side), this requires a transconductance of $G_{m,\text{PA}} = 80$ mS from the amplifier. This $G_{m,\text{PA}}$ includes the ON resistance of the degeneration mixer, designed to be ∼7 Ω. As a result, the transistor g_m

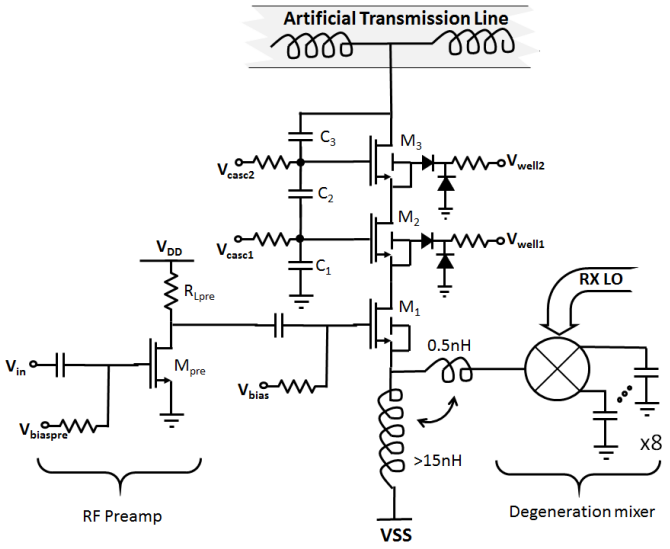

Fig. 8. PA, preamp, and degeneration circuit design. The RF preamp boosts the output of the upconversion mixer. The PA consists of a replica-biased common-source amplifier, with one or two cascodes. The cascode gates are biased to distribute the supply voltage across the transistor's drain–gate junctions, avoiding breakdown. C_1–C_3 ensure that output signal voltage is also evenly distributed. Triple-well devices are used for isolation, with the p-well (body) connected to source, and n-wells biased similar to gates.

needs to be close to 200 mS to achieve the desired overall $G_{m,\mathrm{PA}}$.

Beyond gain and noise, the PA is also designed for high output impedance, since low R_{out} in a distributed amplifier adds shunt loss paths to the TL. Likewise, the individual PAs must withstand large swing on their outputs without their gate oxide breaking down. Therefore, we employed a stacked cascode structure: a single cascode was used in the three PAs closer to the RX and a double cascode for those closer to the antenna where both supply voltage and signal swing are larger. Overvoltage between the drain and gate is mitigated by combining a resistive bias ladder to bias the cascode devices with a capacitive coupling network tied to the drain of each PA as shown in Fig. 8. This allows the gates to move in an ac sense and significantly reduce the swing across the gate–drain junction at a small cost in gain and output impedance.

We used triple-well devices for PA devices, as well as all mixer switches. For PAs, we tied p-bulk to the source and the deep NW to ground (for the input device and mixers) or a resistive ladder (for the cascodes) so that junctions stayed reversed biased and reverse bias never exceeded 3.5 V, even when VSS was pulled below ground. For ESD on the PA source node, we have a diode to ground to protect against positive excursions, and the PA itself should selfprotect against moderate negative ESD excursions.

C. Artificial Transmission Line Design

The TL is composed of series-L/shunt-C sections, integrated on-chip, where $L = 2$ nH and $C = 800$ fF, to provide the desired 50-Ω characteristic impedance and a broadband impedance match. We use MIM capacitors on intermediate segments, and the PA's parasitic drain capacitance as the capacitor to ground on PA-driven segments. Two LC sections per stage were found to provide sufficient delay (80 ps) while keeping the intrinsic cutoff frequency $1/(LC)^{1/2}$ above 4 GHz, this was chosen to ensure that high-frequency performance was not limited by the TL, and so represents factor-of-2 overdesign for the frequency range we achieved. Simulations indicate that for these choices, the system should ideally maintain ∼40 dB of rejection for ±10 MHz BW around center frequencies from 500 MHz to 3 GHz. Our on-chip inductors were simulated to achieve $Q > 10$ across the frequency range of interest.

D. Degeneration Design

The RX-tracking degeneration consists of two elements (Figs. 3 and 8): a passive mixer to provide a narrow-band high impedance at the RX frequency, and a parallel choke inductor to provide a dc path for the PA's bias current. This inductance need not be high-Q, allowing a relatively high value on-chip inductance of 10–15 nH (10 nH at 500 MHz and 15 nH at 2.5 GHz) with a dc resistance of about 8 Ω, for a 250-mV dc drop at maximum bias current. The degeneration choke inductor of each sub-PA is connected directly to its own bond-pad to take advantage of additional bond wire, package, and board-level inductance.

With an eight-phase passive mixer, one would ideally see a degeneration impedance roughly 19.8 times the out-of-band impedance (see Section II). Practically, however, this ratio assumes a broadband impedance presented to the mixer which is constant even at higher (seventh, ninth, and so on) harmonics of the RX LO frequency. Parasitic capacitance on the RF port will act to shunt harmonics, reducing this ratio [21]. By including a small (∼500 pH) series inductance, the impedance at the harmonics is boosted, enhancing A_{deg} [22]. Even further enhancement was achieved by cowinding this low-value high-Q inductor with the high value, low-Q choke inductor, providing a combined improvement of 2–3 dB. Simulations indicated that this composite degeneration structure provided a 14-dB notch in noise coming from the PA in the RX band compared with out-of-band (see Fig. 9).

E. LO Distribution

Eight-phase passive mixers require 12.5% duty-cycle LO pulses [21], [23] with a fixed phase relationship to ensure the desired performance. The LO signals should also have low, correlated phase noise to take maximum advantage of the suppression of correlated noise at the receiver port. The six subtransmitters, therefore, need to share two common LOs (one for upconversion at ω_{TX} and one for degeneration at ω_{RX}). However, 12.5% duty-cycle, sub-1 ns pulses, if distributed across circuits that are millimeters apart will be badly degraded due to the dispersion in the wires [25].

In order to avoid distributing 12.5% duty cycle LO signals across the chip, we instead generated 45° phase-split 50% duty-cycle signals from a shared Johnson counter, and then distributed those signals and the original LO signals to retimer circuitry in each subtransmitter, as shown in Fig. 10. The retimer is a state machine in dynamic CMOS logic, as shown in Fig. 11. Briefly, each retimer receives a phase-split divider output "div," whose rising edge puts the circuit in a sensitive

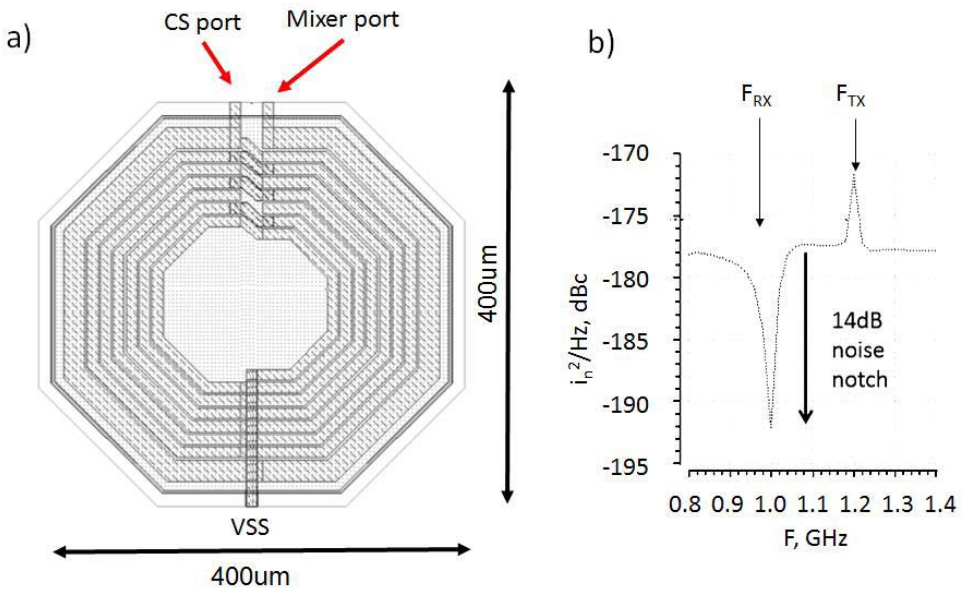

Fig. 9. Degeneration details. (a) Layout of choke inductor and mutual mixer inductor. (b) PSS simulation showing 14-dB enhancement of PA noise with mixer-based degeneration.

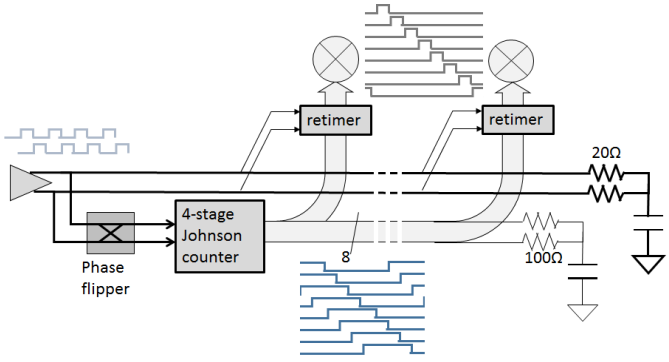

Fig. 10. Distributed LO system. Differential 4X LO signals ("*clk*") are buffered, and drive a four-stage Johnson counter to generate 8, 45°-split square waves. These ten signals are distributed to local retime circuits in each subtransmitter to generate 12.5% duty-cycle LO pulses. A "phase flipper" allows shifting of divided down signal to avoid race conditions in the retimers.

state. The output of the retime (which drives one mixer switch's gate) then rises with the next rising edge of "*clk*," the 4X LO signal, and falls with the next falling edge of "*clk*" (also the rising edge of $\overline{clk}$). After this single pulse, the output stays low until reset by the falling and subsequent rising edges of "*div*," generating a 12.5% duty-cycle pulse with the same relative phase and frequency as "*div*."

This approach provides several benefits: 1) the precise timing of the edges of the output pulse depend only on the timing (and phase noise) of the 4X frequency LO signals; 2) function is insensitive to the precise relative timing of *clk* and *div* except for a race condition at certain frequencies, which are resolved by a "sign flip" control on *clk* and $\overline{clk}$ (see Fig. 10); 3) only a few transistors buffer *clk* to the output, so only these transistors must be sized for low noise; and 4) distributed LO signals are 50% duty cycle, making the circuit resistant to dispersion in their distribution across subtransmitters. The long LO distribution lines were terminated by physical resistors to prevent undesired reflections.

F. Receiver Design

The receiver is similar to that reported in [23] but with the new LO retiming scheme described earlier. It provides an eight-phase output from four differential amplifiers, driven by the eight output phases of the downconversion mixer, loaded by eight large, programmable capacitors to ground. Gain, bandwidth, and feedback impedance are programmable. Circuitry is included to modulate and cancel LO leakage at the RF port as in [24].

IV. Measurement Results

The transceiver was fabricated in a 65-nm CMOS process, and measures 2.4 mm × 3.0 mm, as in Fig. 12. It operates across a wide frequency range of more than 0.3–1.6 GHz. The system in the higher frequencies is limited by the LO performance—generating eight nonoverlapping 12.5% duty cycle pulses becomes more challenging as the frequencies increase. Faster dividers and pulse generators, especially with decreasing feature size should extend this range. The transceiver consumes 2.2 W while transmitting 16 dBm at 900 MHz and receiving at 785 MHz. The PAs consume a total of 600 mW from a 2.5-V VDD and −2.5-V VSS. The LO circuits, due to noise requirements, consume a total of 800 mW from a 1.2-V supply, and the TX baseband circuitry and RF preamplifiers consume 700 mW from a 2.5-V supply. The RX baseband consumes less than 100 mW from 2.5 V. An unexpected (and unmodeled) flaw in which the n-well of the deep-n-well mixer switches were connected to GND instead of VDD prevented raising the bulk voltage above 0.6 V. Since the gate and bulk voltages were referenced from the same source, the gate bias was lowered. This flaw limited the overdrive on the RX downconversion and TX upconversion mixers' gates, significantly increasing their ON resistance, degrading noise, linearity, and signal amplitude.

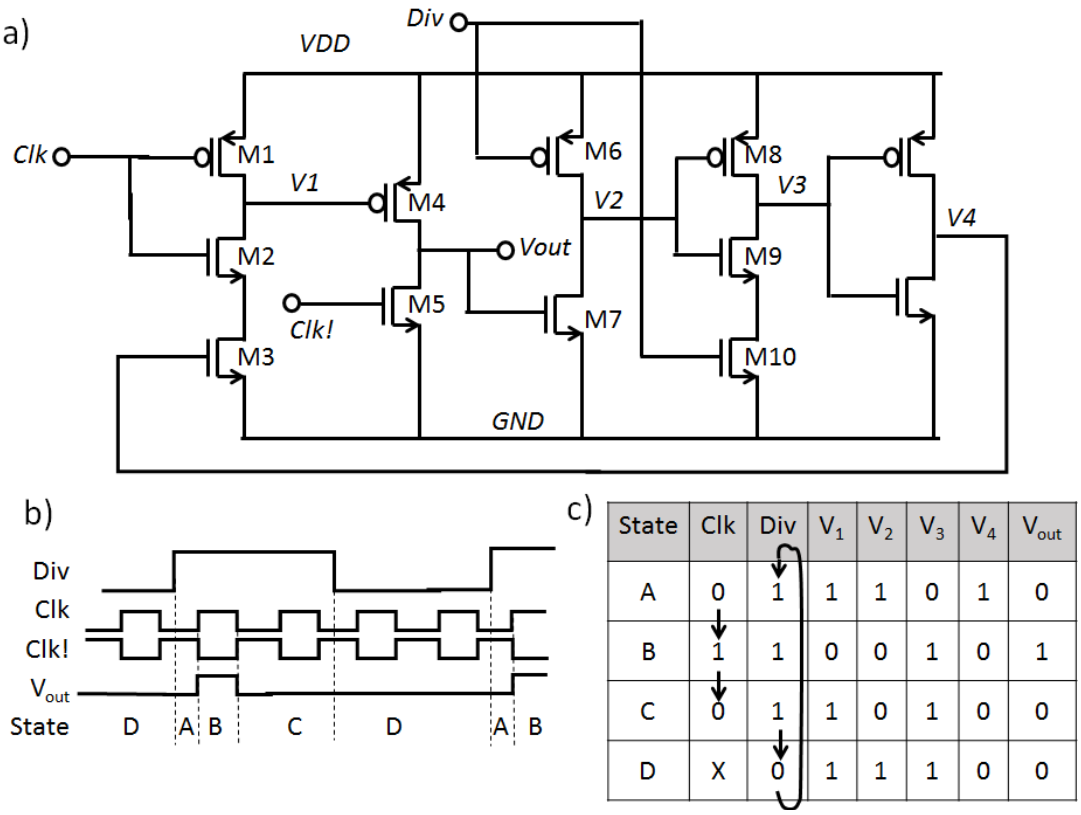

State	Clk	Div	V_1	V_2	V_3	V_4	V_{out}
A	0	1	1	1	0	1	0
B	1	1	0	0	1	0	1
C	0	1	1	0	1	0	0
D	X	0	1	1	1	0	0

Fig. 11. Dynamic LO retime and pulse generator. (a) Transistor-level circuit of pulse generation state machine, only M1–M5 contribute to phase noise. (b) Timing diagram showing sequence of four states, V_{out} and critical edges of *clk* and *div*. (c) Internal voltages in each state.

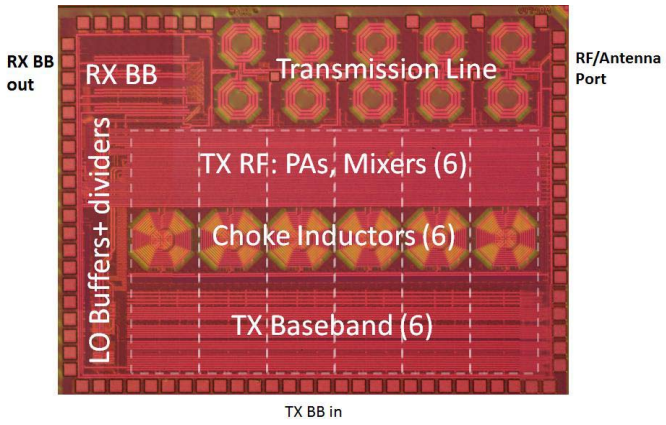

Fig. 12. Die photo.

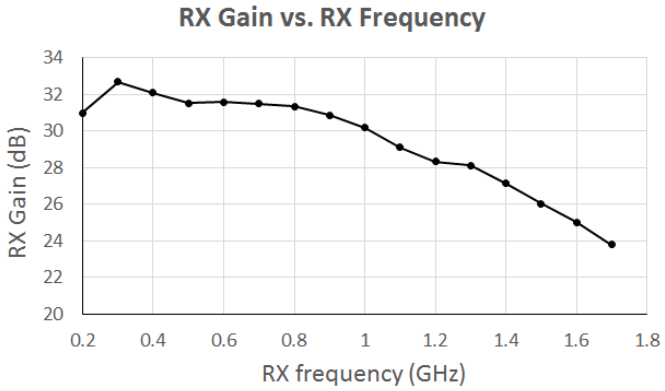

Fig. 13. Measured RX gain across frequency.

A. Basic Receiver Performance

As shown in Fig. 13, the receiver gain was between 24 and 32 dB over the range 200 MHz–1.7 GHz. At 8–12 dB, the RX NF (in Fig. 14) was 4–5 dB worse than expected from simulation and previous work [20] even accounting for the loss of the TL (about 1.5 dB at 700 MHz). A 0 dBm blocker at 700 MHz for a 600-MHz receive signal compressed the receiver by about 3 dB, as shown in Fig. 15. Again, this is worse than expected: the degraded noise and linearity are both likely due to the underdrive of the mixer and associated a much higher R_{sw} value [21].

B. Duplexing Performance

In TDD transmit mode (sub-TXs weighted to protect the receiver, but RX tracking degeneration mixer switches all turned ON for minimum resistance), the transceiver reaches a peak output level of 19.5 dBm and 18% PA drain efficiency. The output level was >14 dBm across the 0.3–1.6 GHz range, with >25 dB of TX suppression at RX (see Fig. 16). Signal levels were likely limited by under drive in the upconversion mixers, rather than the PAs themselves.

Since many duplexers' isolation is sensitive to antenna impedance, we explored the effects of changing VSWR.

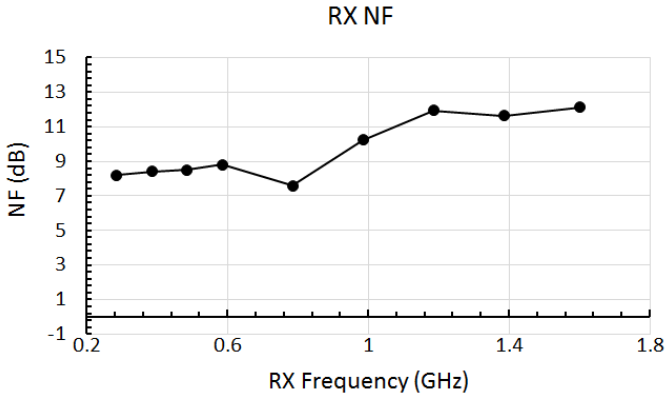

Fig. 14. Measured RX noise figure across frequency.

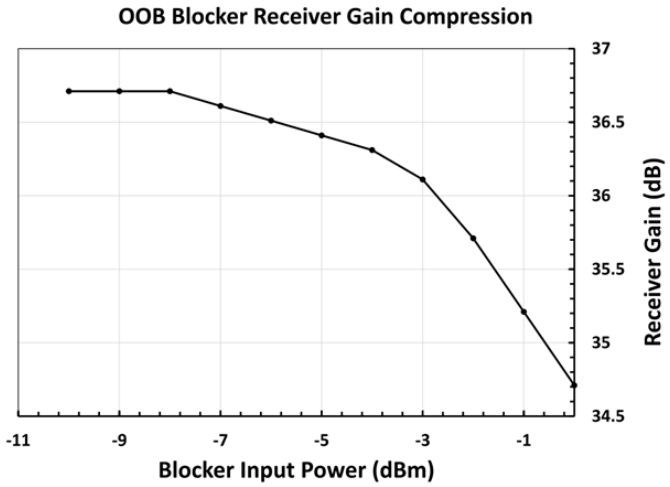

Fig. 15. Measured out-of-band blocker-induced RX gain compression.

As shown in Fig. 17, we changed the RF port impedance for a 3:1 VSWR. This degraded the RX isolation by about 20 dB, and the output power by 5.4 dB. Recomputing the weights for the new impedance, recovered 2 dB in P_{out}, and fully restored TX–RX isolation. TX-induced RX compression also recovered dramatically from recalibration of weights.

TX–RX isolation was moderately sensitive to nonlinear effects, especially at lower frequencies. Optimizing weights for P_{out} at -3 dB back-off, and then increasing to maximum P_{out} degraded TX–RX isolation by less than 8 dB and for frequencies of 600 MHz and above isolation stayed above 20 dB, and could be retuned to better than 25 dB with a slight adjustment to the weights.

C. Degeneration Performance

As seen in Fig. 18, activating degeneration in the PAs reduced PA output power by 3–4 dB, but had little effect on isolation. To confirm the narrow-band effect of RX-tracking degeneration on $G_{m,\text{PA}}$, we injected a small TX input signal, and measured the output level as we swept ω_{RX} relative to ω_{TX} either with the degeneration mixer switches all ON (inactivating the degeneration effect) or acting as an eight-phase mixer. Fig. 19 shows gain reduction across the band by $\sim$4 dB, with further suppression by $>$9 dB for ω_{RX}

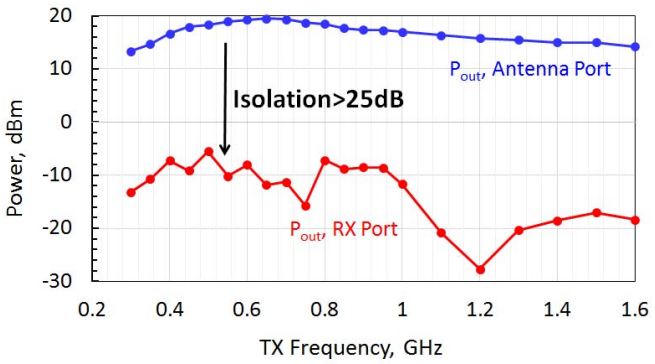

Fig. 16. TX power at antenna port and RX port across frequency, degeneration OFF.

close to ω_{TX}. We also confirmed degeneration's impact on noise and shunting loss by comparing RX NF and gain when degeneration was ON and OFF, across TX signal strength. As can be seen in Figs. 20 and 21, degeneration impacted NF by $>$13 dB, and gain by 1.5 dB.

Finally, we measured RX NF from 185–1615 MHz under three conditions: with TX OFF, with TX ON at moderate power, and TX ON with maximum output power. Degeneration was activated when the TX was ON, and our results are shown in Fig. 22. With the TX OFF, the RX NF was 8–12 dB. In simulation, the NF is much less. We see of 3–4 dB from the receiver and 0.5 dB from the TL. We attribute the discrepancy to the design flaw described earlier, causing an overall increase of 5–8 dB. However, when the transmitter was fully biased, NF degraded by about 4–5 dB due to TX noise being injected into the RX band. Degradation due to this mechanism was worse at band edges. At high frequencies, the degeneration circuit likely underperformed due to reduced swing of the LO, and at low frequencies, ac-coupling degraded LO amplitude, while the degeneration choke inductor's impedance was low enough to shunt the impedance presented by the degeneration mixer. At maximum TX power, NF was degraded by an additional 2–3 dB midband, but much more at the band edges. We attribute this additional degradation to the same reduced LO swing, with the added problem of the degeneration mixer becoming overloaded by large TX signals. Addressing this overload will be an important aspect of future work.

V. Conclusion

In this paper, we have presented a new type of flexible, programmable transceiver that is capable of TDD and FDD with single antenna for RX and TX, across a tuning range of 0.3–1.6 GHz. In TDD mode, the transmitter was able to achieve a transmit power level $>$19 dBm. In FDD mode with active degeneration, TX power was as high as 15.5 dBm with $>$25 dB of TX–RX isolation. We discussed the methods to compute complex weights to achieve this isolation figure.

Eight-phase passive mixers were used for TX upconversion, RX downconversion, and degeneration. The RX NF during FDD operation was degraded by only 4 dB relative to the RX only NF as expected. While a design flaw means that the performance of this prototype was slightly degraded relative

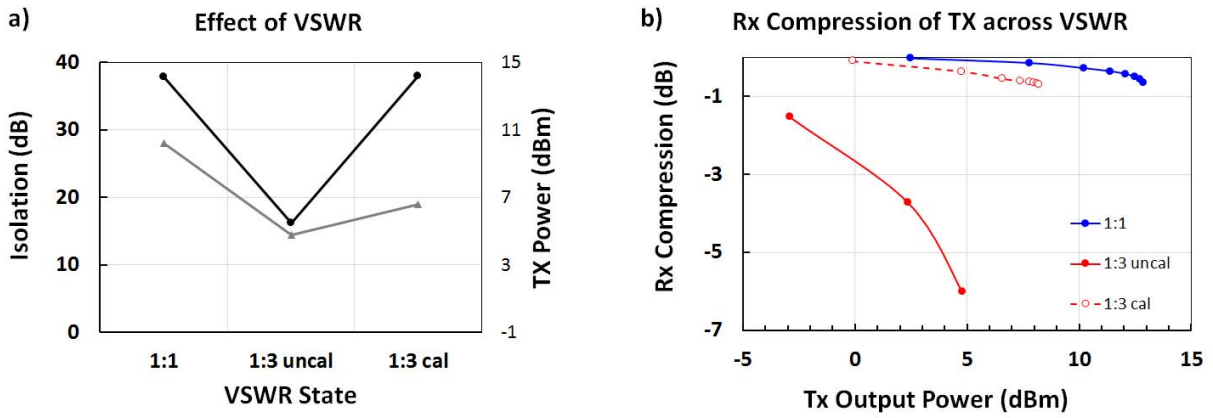

Fig. 17. (a) Effect of changing VSWR on output power and isolation, before and after recomputing TX weights to account for changed Z_{ant}. (b) Effect of TX output power and VSWR on RX gain compression.

TABLE I
PERFORMANCE COMPARISON

Parameter	[10]	[14]	[16]	[17]	[18]	**This Work**
Technology	65nm	90nm	40nm	65nm	65nm	65nm
Duplex RX IL	2.9dB	2.9dB	2.9dB	2.5dB	4.4dB	0dB
Isolation in RX Band	>20dB	>50dB	>50dB	>45dB	>49dB	30dB
RX NF	4.8dB	5.9dB[a]	6.1dB[a]	5.0dB[a]	~6dB	7dB
Frequency Range	0.8-1.4GHz	1.7-2.2GHz	1.5-2.4GHz	3G/4G I, II, III, IV, IX	710-970MHz	0.3-1.5GHz

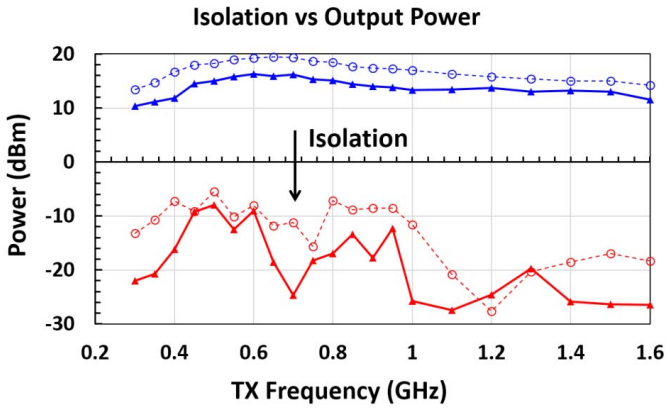

Fig. 18. Effect of RX-tracking degeneration on TX power at antenna port and RX port across frequency, degeneration ON (solid curve) or OFF (dashed curve).

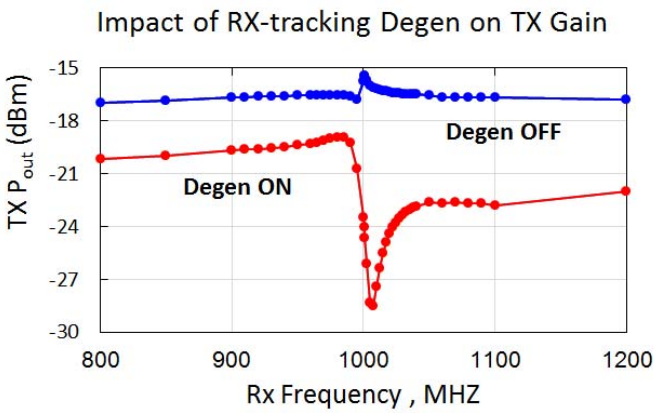

Fig. 19. Effect of RX-tracking degeneration on TX power as a function of RX frequency (TX frequency set at 1000 MHz).

to other approaches to integrated duplex (see Table I), the presented approach provides a significantly wider tuning range while maintaining acceptable isolation, and has significant potential for further improvements.

This paper also reveals several areas for further development, besides the obvious need to fix the flaw in the mixers. In particular, while this paper clearly demonstrates the utility the adaptive distributed duplex, the approach here assumes a narrow-band signal passing through a linear circuit. Future work must pursue circuits and algorithms that enable adaptation for wider band signals and enable distributed digital predistortion to account for nonuniform nonlinear effects across the transmitter stages.

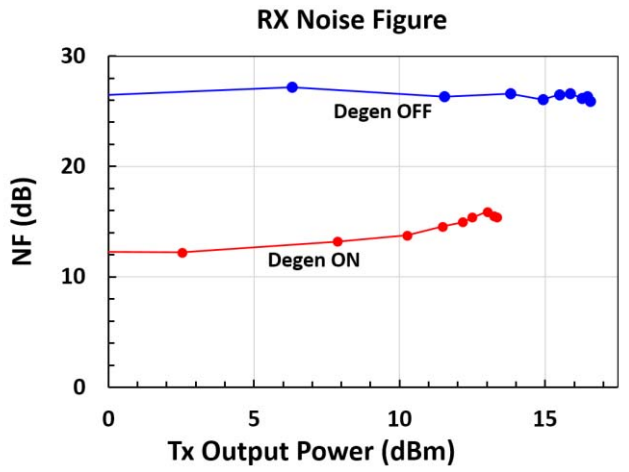

Fig. 20. Effect of RX-tracking degeneration on RX NF versus TX P_{out}. $f_{\text{TX}} = 1$ GHz and $f_{\text{RX}} = 885$ MHz.

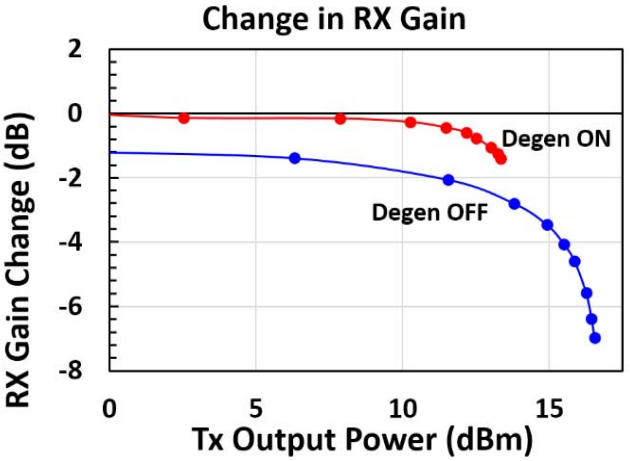

Fig. 21. Measured effect of RX-tracking degeneration on RX gain across TX output power. $f_{\text{TX}} = 1$ GHz and $f_{\text{RX}} = 885$ MHz.

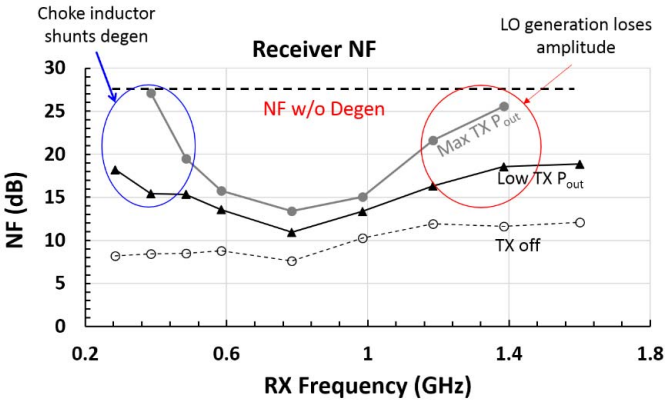

Fig. 22. Measured effect of TX state ON RX NF across frequency, for low and maximum output power. RX NF with TX OFF is shown for comparison.

REFERENCES

[1] M. Ingels *et al.*, "A 5 mm^2 40 nm LP CMOS transceiver for a software-defined radio platform," *IEEE J. Solid-State Circuits*, vol. 45, no. 12, pp. 2794–2806, Dec. 2010.

[2] J. Craninckx *et al.*, "A fully reconfigurable software-defined radio transceiver in 0.13μm CMOS," in *IEEE Int. Solid-State Circuits Conf. (ISSCC) Dig. Tech. Papers*, Feb. 2007, pp. 436–439.

[3] B. Analui, T. Mercer, S. Mandegaran, A. Goel, and H. Hashemi, "A 50 MHz–6 GHz, 2 × 2 MIMO, reconfigurable architecture, software-defined radio in 130nm CMOS," in *Proc. IEEE Radio Freq. Integr. Circuits Symp.*, Jun. 2014, pp. 329–332.

[4] C. Andrews and A. Molnar, "A passive-mixer-first receiver with baseband-controlled RF impedance matching, $\ll$ 6dB NF, and $\gg$ 27dBm wideband IIP3," in *IEEE Int. Solid-State Circuits Conf. (ISSCC) Dig. Tech. Papers*, Feb. 2010, pp. 46–47.

[5] C. Andrews, L. Diamente, D. Yang, B. Johnson, and A. Molnar, "A wideband receiver with resonant multi-phase LO and current reuse harmonic rejection baseband," *IEEE J. Solid-State Circuits*, vol. 48, no. 5, pp. 1188–1198, May 2013.

[6] H. Darabi, A. Mirzaei, and M. Mikhemar, "Highly integrated and tunable RF front ends for reconfigurable multiband transceivers: A tutorial," *IEEE Trans. Circuits Syst. I, Reg. Papers*, vol. 58, no. 9, pp. 2038–2050, Sep. 2011.

[7] M. Mikhemar, H. Darabi, and A. A. Abidi, "A multiband RF antenna duplexer on CMOS: Design and performance," *IEEE J. Solid-State Circuits*, vol. 48, no. 9, pp. 2067–2077, Sep. 2013.

[8] D. Yang *et al.*, "A fully integrated software-defined FDD transceiver tunable from 0.3-to-1.6 GHz," in *Proc. IEEE Radio Freq. Integr. Circuits Symp. (RFIC)*, San Francisco, CA, USA, May 2016, pp. 334–337.

[9] D.-J. van den Broek, E. A. M. Klumperink, and B. Nauta, "A self-interference-cancelling receiver for in-band full-duplex wireless with low distortion under cancellation of strong TX leakage," in *IEEE Int. Solid-State Circuits Conf. (ISSCC) Dig. Tech. Papers*, Feb. 2015, pp. 1–3.

[10] J. Zhou, T.-H. Chuang, T. Dinc, and H. Krishnaswamy, "Receiver with >20MHz bandwidth self-interference cancellation suitable for FDD, co-existence and full-duplex applications," in *IEEE Int. Solid-State Circuits Conf. (ISSCC) Dig. Tech. Papers*, Feb. 2015, pp. 1–3.

[11] D. Yang, H. Yüksel, and A. Molnar, "A wideband highly integrated and widely tunable transceiver for in-band full-duplex communication," *IEEE J. Solid-State Circuits*, vol. 50, no. 5, pp. 1189–1202, May 2015.

[12] The FCC. (Mar. 2008). *Auction 73 700MHz Band*. [Online]. Available: http://wireless.fcc.gov/auctions/default.htm?job=auction_factsheet&id=73

[13] Ericsson. (Mar. 2015). *Mobile Broadband for All: Optimizing Radio Technologies*. [Online]. Available: https://www.ericsson.com/res/docs/whitepapers/mobile-broadband-for-all.pdf

[14] S. H. Abdelhalem, P. S. Gudem, and L. E. Larson, "Hybrid transformer-based tunable differential duplexer in a 90-nm CMOS process," *IEEE Trans. Microw. Theory Techn.*, vol. 61, no. 3, pp. 1316–1326, Mar. 2013.

[15] M. Mikhemar, H. Darabi, and A. Abidi, "An on-chip wideband and low-loss duplexer for 3G/4G CMOS radios," in *Proc. IEEE Symp. VLSI Circuits (VLSIC)*, Jun. 2010, pp. 129–130.

[16] B. van Liempd, B. Hershberg, B. Debaillie, P. Wambacq, and J. Craninckx, "An electrical-balance duplexer for in-band full-duplex with <−85dBm in-band distortion at +10dBm TX-power," in *Proc. 41st Eur. Solid-State Circuits Conf. (ESSCIRC)*, Sep. 2015, pp. 176–179.

[17] J. Zhou, N. Reiskarimian, and H. Krishnaswamy, "Receiver with integrated magnetic-free N-path-filter-based non-reciprocal circulator and baseband self-interference cancellation for full-duplex wireless," in *IEEE Int. Solid-State Circuits Conf. (ISSCC) Dig. Tech. Papers*, Feb. 2016, pp. 178–180.

[18] A. Goel, B. Analui, and H. Hashemi, "Tunable duplexer with passive feed-forward cancellation to improve the RX-TX isolation," *IEEE Trans. Circuits Syst. I, Reg. Papers*, vol. 62, no. 2, pp. 536–544, Feb. 2015.

[19] B. Xiang, X. Wang, and A. B. Apsel, "A reconfigurable integrated dispersive delay line (RI-DDL) in 0.13-μm CMOS process," *IEEE Trans. Microw. Theory Techn.*, vol. 61, no. 7, pp. 2610–2619, Jul. 2013.

[20] B. Xiang, X. Wang, and A. B. Apsel, "On-chip demonstration of real time spectrum analysis (RTSA) using integrated dispersive delay line (IDDL)," in *IEEE MTT-S Int. Microw. Symp. Dig.*, Jun. 2013, pp. 1–4.

[21] D. Yang, C. Andrews, and A. Molnar, "Optimized design of N-phase passive mixer-first receivers in wideband operation," *IEEE Trans. Circuits Syst. I, Reg. Papers*, vol. 62, no. 11, pp. 2759–2770, Nov. 2015.

[22] L. Duipmans, R. E. Struiksma, E. A. M. Klumperink, B. Nauta, and F. E. V. Vliet, "Analysis of the signal transfer and folding in N-path filters with a series inductance," *IEEE Trans. Circuits Syst. I, Reg. Papers*, vol. 62, no. 1, pp. 263–272, Jan. 2015.

[23] C. Andrews and A. C. Molnar, "A passive mixer-first receiver with digitally controlled and widely tunable RF interface," *IEEE J. Solid-State Circuits*, vol. 45, no. 12, pp. 2696–2708, Dec. 2010.

[24] S. Jayasuriya, D. Yang, and A. Molnar, "A baseband technique for automated LO leakage suppression achieving < -80dBm in wideband passive mixer-first receivers," in *Proc. IEEE Custom Integr. Circuits Conf. (CICC)*, Sep. 2014, pp. 1–4.
[25] C. Andrews, C. Lee, and A. Molnar, "Effects of LO harmonics and overlap shunting on N-phase passive mixer based receivers," in *Proc. ESSCIRC*, Bordeaux, France, Sep. 2012, pp. 117–120.
[26] V. Aparin, G. J. Ballantyne, C. J. Persico, and A. Cicalini, "An integrated LMS adaptive filter of TX leakage for CDMA receiver front ends," *IEEE J. Solid-State Circuits*, vol. 41, no. 5, pp. 1171–1182, May 2006.
[27] J. Zhou, A. Chakrabarti, P. R. Kinget, and H. Krishnaswamy, "Low-noise active cancellation of transmitter leakage and transmitter noise in broadband wireless receivers for FDD/co-existence," *IEEE J. Solid-State Circuits*, vol. 49, no. 12, pp. 3046–3062, Dec. 2014.

Hazal Yüksel (S'14) received the B.S. degree in electrical engineering with a minor in mathematics from Duke University, Durham, NC, USA, in 2012. She is currently pursuing the Ph.D. degree in electrical engineering with Cornell University, Ithaca, NY, USA.

Her current research interests include signal processing and adaptive radios.

Dong Yang received the B.S. degree in control science and engineering from Zhejiang University, Hangzhou, China, in 2010, and the Ph.D. degree in electrical and computer engineering from Cornell University, Ithaca, NY, USA, in 2015.

He joined Broadcom Ltd., Sunnyvale, CA, USA, in 2015. Since 2016, he has been with Cypress Semiconductor Corporation, San Jose, CA, USA.

Zachariah Boynton received the B.S. degree in electrical engineering from the University of Massachusetts Amherst, MA, USA, in 2015.

His current research interests include RF, analog, and mixed-signal circuit design.

Changhyuk Lee (S'08–M'14) received the B.S. degree in electrical and computer engineering from Korea University, Seoul, South Korea, in 2005, and the M.S. and Ph.D. degrees from Cornell University, Ithaca, NY, USA. His Ph.D. thesis was on mixed signal integrated circuits design for lensless biomedical sensing devices.

He is currently a Post-Doctoral Research Associate in electrical engineering with Columbia University, New York, NY, USA. His current research interests include optoelectronic neural interfaces, implantable bionics, computational neuroscience, and neurobiology.

Thomas Tapen received the B.S. in electrical engineering from Cornell University, Ithaca, NY, USA, in 2015.

His current research interests include mixed-signal integrated circuit design.

Alyosha Molnar (M'07) received the B.S. degree (Hons.) in engineering from Swarthmore College, Swarthmore, PA, USA, in 1997, and the M.S. and Ph.D. degrees in electrical engineering from the University of California, Berkeley, CA, USA, in 2003 and 2007, respectively.

From 1998 to 2002, he was with the RF IC Group, Skyworks Solutions, Inc., Newport Beach, CA, USA, where he developed their first-generation GSM direct conversion receiver. In 2007, he joined the Faculty of the School of Electrical and Computer Engineering, Cornell University, Ithaca, NY, USA.

Alyssa Apsel (M'03–SM'10) received the B.S. degree from Swarthmore College, Swarthmore, PA, USA, in 1995, and the Ph.D. degree from Johns Hopkins University, Baltimore, MD, USA, in 2002.

She joined Cornell University, Ithaca, NY, USA, in 2002, where she is currently a Professor of electrical and computer engineering. She has authored or co-authored over 100 refereed publications in related fields of RF mixed-signal circuit design, ultralow-power radio, interconnect design and planning, photonic integration, and process invariant circuit design techniques, resulting in eight patents and several pending patent applications. Her current research interests include power-aware mixed-signal circuits and design for highly scaled CMOS and modern electronic systems.

Dr. Apsel received best paper awards at ASYNC in 2006 and the IEEE SiRF in 2012, the College Teaching Award in 2007, and the National Science Foundation CAREER Award in 2004. She was selected by *Technology Review Magazine* as one of the Top Young Innovators in 2004. She had a MICRO Top Picks paper in 2006. She has served as an Associate Editor of various journals, including the IEEE TRANSACTIONS ON CIRCUITS AND SYSTEMS I and II, and has also served as the Chair of the Analog and Signal Processing Technical Committee of ISCAS 2011, as Deputy Editor-in-Chief of the *IEEE Circuits and Systems (CAS) Magazine*, and on the Board of Governors of the IEEE CAS Society.